A coupled-mode model for the scattering of water waves by shearing currents in variable bathymetry

K. A. BELIBASSAKIS†

School of Naval Architecture and Marine Engineering, National Technical University of Athens,
Heroon Polytechniou 9, Zografos 15773, Athens, Greece
kbel@fluid.mech.ntua.gr

A coupled-mode model is presented for wave–current–seabed interaction, with application to the problem of wave scattering by ambient shearing currents in variable bathymetry regions. We consider obliquely incident waves on a horizontally non-homogeneous current in a variable-depth strip, which is characterized by straight and parallel bottom contours. The flow associated with the current is assumed to be directed along the bottom contours and it is considered to be steady and known. In a finite subregion containing the bottom irregularity, we assume that the horizontal current profile is general and smoothly varying. Outside this region, the current is assumed to be uniform (or zero). Based on a variational principle, in conjunction with a rapidly convergent local-mode series expansion of the wave pressure field in the finite subregion containing the current variation and the bottom irregularity, a new coupled-mode system of equations is obtained, governing the scattering of waves in the presence of variable bathymetry and longshore shearing currents. By keeping only the propagating mode in the local-mode series, a new one-equation model is derived, having the property to reduce to the modified mild-slope equation when the current is zero, and to the enhanced mild-shear equation when the bottom is flat. An important aspect of the present model is that it can be further elaborated to treat shearing currents with general, depth-dependent vertical structure, and to include the effects of weak nonlinearity.

1. Introduction

Except of depth variations, the presence of currents significantly influences the propagation of waves in the nearshore and coastal environment. Detailed knowledge of the wave characteristics in the presence of ambient currents and bottom variations is important for various applications, as, for example, in coastal and harbour engineering problems, in the study of oil slick dispersion and pollutant transport in nearshore and coastal waters, as well as for sediment transport and coastal erosion studies. Extensive reviews on the subject of wave–current interaction in the sea and in the nearshore region have been presented by Peregrine (1976), Jonsson (1990) and Thomas & Klopman (1997). Non-homogeneous shearing currents, following or opposing wavetrains, produce significant changes in the wave characteristics, especially in the

† Current address: Technological Educational Institute of Athens, Athens 12210, Greece.

region where there is a rapid change of current strength. Thus, large-amplitude waves may appear as a result of interaction of obliquely propagating waves with adverse currents (see, e.g. Mei 1983; Jonsson 1990, §1B). Wave amplification could be further enhanced by inshore effects due to sloping seabeds, and has sometimes been reported to be connected with the appearance of 'giant waves' in coastal waters (see, e.g. Dysthe 2000; Faulkner 2000).

Wave–current interaction models over slowly varying bottom topography have been developed and studied by various authors. Under the assumption of irrotational wave motion, Kirby (1984) derived a phase-resolving one-equation model, generalizing the mild-slope equation (Berkhoff 1972) in regions with slowly varying depth and ambient currents (see also Liu 1990). The latter model in its elliptic time-harmonic form has been exploited, in conjunction with numerical (finite-element, finite difference etc.) solvers, to numerous wave–current–seabed interaction applications (see, e.g. Chen, Panchang & Demirbilek 2005 and references therein).

On the other hand, if the wave flow is assumed to be weakly rotational, as happens to be the case when waves are scattered by shearing currents characterized by stronger horizontal gradients, McKee (1987) derived another one-equation model, called the mild-shear equation. However, the validity of the mild-shear equation is based on the assumption of slow current and depth variations compared to the typical wavelength. In the case of a flat bottom, the mild-shear model has been further enhanced by McKee (1996) by including an extra term and obtaining the so-called enhanced mild-shear equation. The latter model is applicable to cases where the shearing current is varying on the scale of the wavelength. In McKee (1987, 1996) the current is considered to be flowing along one horizontal direction while the bottom topography varies in the other horizontal direction. Thus, the mild-shear model is more appropriate for problems of wave scattering by slowly varying depth and longshore-type ambient shearing currents.

In both the above approaches (mild-slope model, mild-shear model) the effects of evanescent modes, describing higher-order localized effects due to bottom and current variations, have been ignored. Apart from the above models based on the irrotational and weakly rotational assumption concerning the wave motion, another class of wave–current–seabed interaction models have been developed, applicable to cases where the lateral length scale on which the medium (bottom topography and current) is changing is much smaller than the typical wavelength. In this case, the problem has been modelled by means of step discontinuities and vertical vortex sheets, separating subregions of essentially potential flow, in conjunction with appropriate matching conditions ensuring continuity of pressure and normal flow following the vortex sheet(s). In this context, generalizing the work by Evans (1975) for the transmission of deep-water waves across a vortex sheet, Smith (1983, 1987) presented models treating the problem of waves crossing uniform current jets in constant finite depth and crossing a step with horizontal shear, respectively. Also, Kirby, Dalrymple & Seo (1987) studied the propagation of obliquely incident waves over a trench with uniform current flowing along it. In the latter models, complete representations of the wave potentials in the various subregions have been used, containing both the propagating and the evanescent modes, which are necessary in order to satisfy the matching/boundary conditions at the vertical interfaces (vortex sheets and depth discontinuities). Finally, the approach by Smith (1987) and Kirby *et al.* (1987) has been further exploited by McKee (2003) to study scattering of waves by shearing currents of general horizontal structure in water of constant depth. In the latter work, the current is modelled by a series of vertical vortex sheets separating subregions of constant current velocity, and the solution is again obtained by using complete
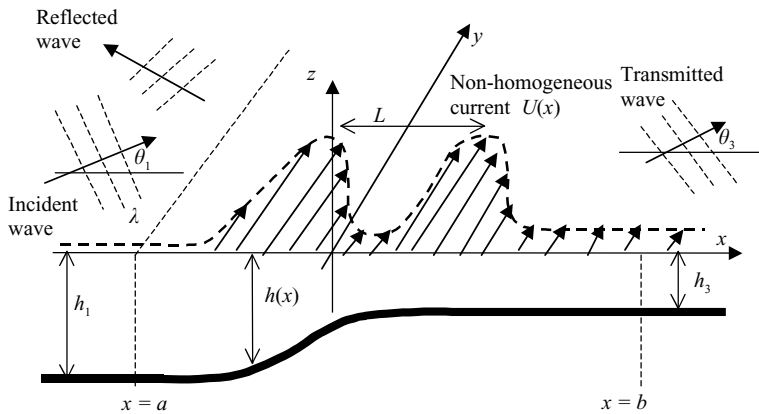
FIGURE 1. Geometrical configuration and basic notation.

representations of the wave potential in each subregion and matching conditions at the vertical interfaces. Also, in McKee (2003) systematic comparisons have been presented between the predictions by the mild-shear equation(s) and the piecewise constant current velocity approximation, which is considered as more exact, showing that the accuracy of the enhanced mild-shear equation is generally better than the original mild-shear equation. Furthermore, it is shown in the same work that in cases of waves interacting with strong adverse shearing currents, as well as in cases where the current variation length is much smaller than the wavelength, the accuracy of the simplified mild-shear models is lost.

In the present work, a continuous coupled-mode model is developed for the scattering of water waves by horizontally shearing currents in variable bathymetry regions, without any asymptotic assumption or restriction concerning the smallness of the bottom and current variation lengths with respect to the local wavelength. We consider obliquely incident harmonic waves on a horizontally non-homogeneous current in a variable-depth strip, characterized by straight and parallel bottom contours (figure 1). For simplicity, the flow associated with the current is assumed to be parallel to the bottom contours and it is considered to be uniform in depth and known. In a finite subregion containing the bottom irregularity, the horizontal current profile is general and smoothly varying. Outside this region, the current is assumed to be uniform (or zero). Under the smallness assumption concerning the steepness of the waves, the problem is governed by the linearized Euler equations, the free-surface and the bottom no-entrance boundary conditions, as described in §2.

The present coupled-mode system of equations on the horizontal plane is obtained by an appropriate variational principle, described in §3, in conjunction with a rapidly convergent local-mode series expansion of the wave pressure field in the finite subregion containing the current variation and the bottom irregularity, discussed in §4. The local-mode series contains, apart from the propagating and evanescent modes, an additional term, called the sloping-bottom mode, first introduced by Athanassoulis & Belibassakis (1999) for the propagation of water waves in variable bathymetry regions. The sloping-bottom mode enables the consistent satisfaction of the Neumann boundary condition on the non-horizontal parts of the bottom, and substantially accelerates the rate of convergence of the local-mode series. Thus, for all practical applications, a small number of modes (of the order of 4–5, including the propagating mode, the sloping-bottom mode and the first few evanescent modes) is found to be enough for an accurate numerical solution. Moreover, by keeping

only the propagating mode in the local-mode series, a new one-equation model has been derived and discussed in §4.2, called the *mild-slope and shear equation*. This new model approximately describes the combined scattering effects due to shearing current and bottom irregularities, and consistently generalizes both the modified mild-slope equation (Massel 1993; Chamberlain & Porter 1995) and the enhanced mild-shear equation (McKee 1996), having the property to reduce exactly to the former when the current is zero and to the latter when the bottom is flat.

Numerical results are presented in §5.1 for the scattering of waves by jet-like shearing currents in constant depth, including comparisons with the multidomain approximation method (McKee 2003), and the simplified mild-shear model(s) (McKee 1987, 1996). It is shown that the present coupled-mode model with a small number of modes provides results fully compatible with the exact multidomain approximation method. Furthermore, with the aid of systematic comparisons in cases of smooth but steep shoals, in §5.2, we present and discuss the effects of transitional-type following and opposing currents on the hydrodynamic characteristics of the wave–current system. As another example, we examine in §5.3 the case of a waves scattered by sinusoidal current in constant depth, and show that there are cases where strong enhancement of the wave amplitude could be obtained within downwave-directed current jets. This is in agreement with previous observations which suggested that wind-wave amplitudes might be enhanced within the downwind-directed current maxima associated with alternating 'wind streaks' or 'Langmuir circulation' (Smith 1983, 2001), leading to preferential breaking of waves along such current jets. Finally, in §5.4, we investigate the influence of longshore-type currents over sinusoidal bottom topography on the Bragg scattering of obliquely incident water waves and discuss their effects on the shifting of the first-order resonant frequencies and the enhancement/reduction of reflection.

2. Differential formulation of the problem

The present work is based on the following differential equation on the wave pressure p, which models the combined effects of steady shearing current and variable bathymetry on small-amplitude waves (Mei 1983, chap. 3.6),

$$\frac{\partial^2 p}{\partial x_i \partial x_i} + \frac{\partial^2 p}{\partial z^2} = -2\rho \left(\frac{\partial u_i}{\partial x_j} \frac{\partial U_j}{\partial x_i} + \frac{\partial w}{\partial z} \frac{\partial W}{\partial z} \right), \tag{2.1}$$

where (u_1, u_2, w) denotes the wave flow and (U_1, U_2, W) the steady current, $(x_1, x_2) = (x, y)$ are the horizontal coordinates and z is the vertical coordinate (positive upwards), and ρ is the (constant) density. Equation (2.1) has been obtained from the continuity equation and the Euler equations, after appropriate linearization. Furthermore, the wave pressure should satisfy the linearized free-surface boundary condition,

$$\left(\frac{\partial}{\partial t} + U_j \frac{\partial}{\partial x_j} \right)^2 p + 2W \left(\frac{\partial p}{\partial t} + U_j \frac{\partial P}{\partial x_j} \right) - g \frac{\partial H}{\partial x_j} \frac{\partial p}{\partial x_j} + g \frac{\partial p}{\partial z} = 0 \quad \text{on} \quad z = H, \tag{2.2}$$

where P and H denote the pressure and the free-surface elevation associated with the (underlying) steady current flow and g is the acceleration due to gravity, as well as the kinematic boundary condition

$$\frac{\partial \eta}{\partial t} + U_i \frac{\partial \eta}{\partial x_i} + u_i \frac{\partial H}{\partial x_i} - w - \eta \frac{\partial W}{\partial z} = 0 \quad \text{on} \quad z = H, \tag{2.3}$$

where η detotes the free-surface elevation associated with the wave flow. Also, the wave pressure p must satisfy the bottom boundary condition, which reads

$$\frac{\partial p}{\partial z} + \frac{\partial h}{\partial x_j}\frac{\partial p}{\partial x_j} = 0 \quad \text{on} \quad z = -h. \tag{2.4}$$

In the present work, we consider a simplified model problem corresponding to obliquely incident harmonic waves on a horizontally non-homogeneous current in a variable-depth strip, characterized by straight and parallel bottom contours (figure 1). The liquid is assumed to be homogeneous, and the flow associated with the current is parallel to the bottom contours and it is considered to be steady and known. More specifically, the bottom surface exhibits an arbitrary one-dimensional variation in a subdomain of finite length (i.e. the bathymetry is characterized by straight and parallel bottom contours) lying between two regions of constant but possibly different depth, $h = h_1$(region of incidence) and $h = h_3$ (region of transmission). The function $h(x)$ represents the local depth, measured from the mean water level. It is considered to be a smooth function, such that $h(x) = h(a) = h_1$ for $x \leqslant a$, and $h(x) = h(b) = h_3$ for $x \geqslant b$. The vertical strip D is decomposed into three subdomains $D^{(i)}$, $i = 1, 2, 3$, where $D^{(1)}$ and $D^{(3)}$ are half-strips, corresponding to $x < a$ and $x > b$, respectively, and $D^{(2)}$ is the variable bathymetry subdomain lying between $D^{(1)}$ and $D^{(3)}$. The same decomposition is also applied to the free-surface and the bottom boundaries.

We consider the scattering problem of obliquely incident plane waves, under the combined effects of variable bathymetry and the horizontally non-homogeneous shear current, $U_1 = W = 0$, $U_2 = U(x)$, existing only in $x > a$ (figure 1). The steady current set-down is assumed to be negligible ($H = 0$), and thus, also $P = 0$. The current velocity is described by the differentiable function $U(x)$, which can be general in the intermediate region, $a \leqslant x \leqslant b$, as, for example, a monotonic one or a periodic one with characteristic length L. Outside this region, the current is assumed to be uniform (or simply zero),

$$U(x) = U_1 = 0, \quad x \leqslant a, \quad U(x) = U_3, \quad x \geqslant b. \tag{2.5}$$

Restricting ourselves to monochromatic (harmonic) waves of absolute frequency ω, propagating with direction θ_1 with respect to the bottom contours in the region of incidence, the wave pressure is expressed in the form (Smith 1983, 1987),

$$p(x, y, z; t) = \text{Re}\{p(x, z) \exp(i(qy - \omega t))\}, \tag{2.6}$$

where q is the periodicity constant along the $y-$direction and $i = \sqrt{-1}$. Under the previous assumptions, from (2.1), (2.2) and (2.4) we find that the wave flow is governed by the following equation with respect to the (complex) pressure $p(x, z)$ in D,

$$\frac{\partial^2 p}{\partial x^2} + \frac{\partial^2 p}{\partial z^2} - q^2 p + \frac{2q}{\sigma}\frac{\partial U}{\partial x}\frac{\partial p}{\partial x} = 0, \tag{2.7a}$$

subjected to the boundary conditions

$$\frac{\partial p}{\partial z} - \mu(x)\, p = 0 \quad \text{on} \quad z = 0, \tag{2.7b}$$

$$\frac{\partial p}{\partial z} + \frac{dh}{dx}\frac{\partial p}{\partial x} = 0 \quad \text{on} \quad z = -h(x), \tag{2.7c}$$

where $\sigma = \sigma(x) = \omega - qU(x)$ is the local intrinsic frequency and $\mu = \sigma^2/g$ is the corresponding frequency parameter.

Following (2.3), the free-surface elevation can be obtained from the solution of the above problem as follows

$$\eta(x, y; t) = \mathrm{Re}\left\{\frac{p(x, z = 0)}{\rho g}\exp\left(\mathrm{i}(qy - \omega t)\right)\right\}. \tag{2.8}$$

Other quantities of interest, as, for example, the wave velocities, can be obtained in terms of $p(x, z)$ and its spatial derivatives from the linearized Euler equations (Mei 1983, equations (6.15) and (6.16)) as follows:

$$u_1 = -\frac{\mathrm{i}}{\rho\sigma}\frac{\partial p}{\partial x}, \quad u_2 = -\frac{\mathrm{i}q}{\rho\sigma}p - \frac{1}{\rho\sigma^2}\frac{\partial U}{\partial x}\frac{\partial p}{\partial x}, \quad w = -\frac{\mathrm{i}}{\rho\sigma}\frac{\partial p}{\partial z}. \tag{2.9}$$

The problem of water-wave scattering by the shearing current $U(x)$, with the effects of variable bathymetry, can be formulated as a transmission problem in the bounded subdomain $D^{(2)}$, with the aid of the following general representations of the pressure $p(x, z)$ in the semi-infinite strips $D^{(1)}$ and $D^{(3)}$ (Smith 1983, 1987; Kirby et al. 1987):

$$p^{(1)}(x, z) = \left(A_0\exp\left(\mathrm{i}k_0^{(1)}x\right) + A_R\exp\left(-\mathrm{i}k_0^{(1)}x\right)\right)Z_0^{(1)}(z) + \sum_{n=1}^{\infty}C_n^{(1)}Z_n^{(1)}(z)\exp\left(k_n^{(1)}(x-a)\right), \tag{2.10a}$$

in $D^{(1)}$, where A_0 is the amplitude of the (known) incident wave, and

$$p^{(3)}(x, z) = A_T\exp\left(\mathrm{i}k_0^{(3)}x\right)Z_0^{(3)}(z) + \sum_{n=1}^{\infty}C_n^{(3)}Z_n^{(3)}(z)\exp\left(k_n^{(3)}(b-x)\right) \text{ in } D^{(3)}. \tag{2.10b}$$

The above expansions are obtained from the eigensolutions of the modified Helmholtz equation to which (2.7a) reduces in $D^{(1)}$ and $D^{(3)}$ (since $\mathrm{d}U/\mathrm{d}x = 0$ there). The terms $(A_0\exp(\mathrm{i}k_0^{(1)}x) + A_R\exp(-\mathrm{i}k_0^{(1)}x))Z_0^{(1)}(z)$ and $A_T\exp(\mathrm{i}k_0^{(3)}x)Z_0^{(3)}(z)$ in the series (2.10) are the propagating modes, associated with incident wave (which is considered to be known), the reflected and the transmitted wave, respectively. The remaining terms $(n = 1, 2, \ldots)$ are the evanescent modes. In (2.10), the horizontal wavenumbers $k_n^{(l)}$, $l = 1, 3$, are defined as follows

$$k_0^{(l)} = \sqrt{\left(\kappa_0^{(l)}\right)^2 - q^2}, \quad k_n^{(l)} = \sqrt{\left(\kappa_n^{(l)}\right)^2 + q^2} \quad (n \geqslant 1), \tag{2.11a}$$

where $\{\mathrm{i}\kappa_0^{(i)}, \kappa_n^{(i)}, \ n = 1, 2, \ldots\}$, $l = 1, 3$, are obtained as the roots of the dispersion relations (formulated at the depths h_l, $l = 1, 3$):

$$\mu_l h_l = -\kappa^{(l)}h_l\tan\left(\kappa^{(l)}h_l\right) \quad (l = 1, 3). \tag{2.11b}$$

In the above equations $\mu_l = \sigma_l^2/g$, $\sigma_l = \omega - qU_l$, $l = 1, 3$. Also, the functions $\{Z_n^{(l)}(z), \ n = 0, 1, 2, \ldots\}$ appearing in (2.10) are given by

$$Z_0^{(l)}(z) = \frac{\cosh\left(\kappa_0^{(l)}(z + h_l)\right)}{\cosh\left(\kappa_0^{(l)}h_l\right)}, \quad Z_n^{(l)}(z) = \frac{\cos\left(\kappa_n^{(l)}(z + h_l)\right)}{\cos\left(\kappa_n^{(l)}h_l\right)} \quad (n = 1, 2, \ldots, \ l = 1, 3). \tag{2.12}$$

Since the current is assumed to be zero in $D^{(1)}$, the intrinsic and absolute frequencies are equal there $(\sigma = \omega)$. Thus, the periodicity constant q is obtained from the wavenumber of the incident wave, as follows

$$q = \kappa_0^{(1)}\sin\theta_1, \tag{2.13}$$

where $\mathrm{i}\kappa_0^{(1)}$ is the unique imaginary-positive root of (2.11b) for $l = 1$. Then, the direction

of the transmitted wave in $D^{(3)}$ is calculated by

$$\theta_3 = \sin^{-1}\left(\kappa_0^{(1)}\sin\theta_1/\kappa_0^{(3)}\right), \tag{2.14}$$

where $i\kappa_0^{(3)}$ is the unique imaginary-positive root of (2.11b) for $l=3$. An important property of the solution $p(x,z)$ to (2.7) (see also McKee 1987, §3) is that it satisfies the conservation of wave action flux through vertical sections in the strip D,

$$\frac{1}{\sigma^2(x)}\int_{z=-h(x)}^{z=0}\mathrm{Im}\left(\bar{p}(x,z)\frac{\partial p(x,z)}{\partial x}\right)\mathrm{d}z = \mathrm{const} \quad \text{for all } x, \tag{2.15a}$$

where an overbar denotes the complex conjugate. Application of (2.15a) to the regions of incidence $D^{(1)}$ and transmission $D^{(3)}$ away from the inhomogeneity ($x \to \pm\infty$), in conjunction with representations (2.10) keeping only the corresponding propagating ($n=0$) modes, and using

$$\int_{z=-h_l(x)}^{z=0}\left(Z_0^{(l)}(z)\right)^2\mathrm{d}z = \frac{1}{g}\frac{\sigma_l}{\kappa_0^{(l)}}(C_g)_l, \quad l = 1, 3,$$

results in

$$\left(|A_0|^2 - |A_R|^2\right)\frac{(C_g)_1\cos\theta_1}{\sigma_1} = |A_T|^2\frac{(C_g)_3\cos\theta_3}{\sigma_3}, \tag{2.15b}$$

where $(C_g)_l$, $l=1,3$, denote the group velocities in $D^{(1)}$ and $D^{(3)}$. Since the terms $(|A_0|^2 - |A_R|^2)$ and $|A_T|^2$ are proportional to the wave energy in the regions of incidence and transmission, respectively, (2.15b) is recognized as the integral form of wave action conservation law in the present case (Smith 1983, §3; Mei 1983, equation (7.14)). Moreover, (2.15b) provides us with an expression connecting the reflection and transmission coefficients that can be used to check the accuracy of any numerical solution.

Given the representations (2.10), the problem can be reformulated as a transmission boundary-value problem for the wave pressure, consisting of (2.7a–c) for $p(x,z)$ in the bounded subdomain $D^{(2)}$, in conjunction with the matching conditions:

$$p = p^{(1)}, \qquad \frac{\partial p}{\partial x} = \frac{\partial p^{(1)}}{\partial x}, \quad x = a, \quad -h_1 < z < 0, \tag{2.16a,b}$$

$$p = p^{(3)}, \qquad \frac{\partial p}{\partial x} = \frac{\partial p^{(3)}}{\partial x}, \quad x = b, \quad -h_3 < z < 0, \tag{2.16c,d}$$

on the vertical interfaces $\partial D_I^{(12)}(x=a)$ and $\partial D_I^{(23)}(x=b)$ separating the three subdomains.

3. Variational formulation

The transmission problem admits an equivalent variational formulation, which will be used in the sequel for the derivation of a new coupled-mode system governing the scattering of waves by horizontally shearing current in variable bathymetry regions. Consider the functional:

$$\mathcal{F}\left(p, A_R, \{C_n^{(1)}\}_{n\in N}, A_T, \{C_n^{(3)}\}_{n\in N}\right) = \frac{1}{2}\int_{D^{(2)}}\left(\nabla\left(\frac{p}{\sigma}\right)\right)^2 + \left(q^2 + \sigma\frac{\partial^2\sigma^{-1}}{\partial x^2}\right)\left(\frac{p}{\sigma}\right)^2\mathrm{d}x\,\mathrm{d}z$$

$$-\frac{1}{2}\int_{\partial D_F^{(2)}}\mu\left(\frac{p}{\sigma}\right)^2\mathrm{d}S - \frac{1}{2}\int_{\partial D_\Pi^{(2)}}\left(\sigma\frac{\partial}{\partial n}\left(\frac{1}{\sigma}\right)\right)\left(\frac{p}{\sigma}\right)^2\mathrm{d}S + \frac{1}{\sigma_1^2}\int_{\partial D_I^{(12)}}\left(p - \tfrac{1}{2}p^{(1)}\right)\frac{\partial p^{(1)}}{\partial x}\mathrm{d}S$$

$$-\frac{1}{\sigma_3^2}\int_{\partial D_I^{(23)}}\left(p - \tfrac{1}{2}p^{(3)}\right)\frac{\partial p^{(3)}}{\partial x}\mathrm{d}S - A_0 A_R J^{(1)}, \tag{3.1}$$

where,

$$J^{(1)} = 2k_0^{(1)} \int_{z=-h_1}^{z=0} \left(Z_0^{(1)}(z) \right)^2 \mathrm{d}z,$$

$\sigma_1 = \sigma(x = a)$ and $\sigma_3 = \sigma(x = b)$, $\partial/\partial n$ denotes the outward normal derivative on the boundary and $\nabla = (\partial/\partial x, \ \partial/\partial z)$. In (3.1) $\partial D_F^{(2)}$ denotes the free surface ($z = 0$) and $\partial D_\Pi^{(2)}$ the bottom surface ($z = -h$). The functions $p^{(l)}$ and their derivatives $\partial p^{(l)}/\partial x$, $l = 1, 3$, appearing in (3.1), are considered to be represented by means of their series expansions, (2.10), and their horizontal derivatives, respectively.

The function $p = p^{(2)}(x, z)$, $(x, z) \in D^{(2)}$ and the coefficients A_R, $\{C_n^{(1)}\}_{n \in N}$ and A_T, $\{C_n^{(3)}\}_{n \in N}$ constitute a solution of the problem, if they render the functional $\mathcal{F}$ stationary, $\delta \mathcal{F} = 0$. By calculating the first variation of the above functional we obtain the variational equation:

$$-\int_{D^{(2)}} \frac{1}{\sigma^2} \left(\nabla^2 p - q^2 p + \frac{2q}{\sigma} \frac{\partial U}{\partial x} \frac{\partial p}{\partial x} \right) \delta p \, \mathrm{d}x \, \mathrm{d}z + \int_{x=a}^{x=a} \frac{1}{\sigma^2} \left(\frac{\partial p}{\partial z} - \mu p \right) \delta p \, \mathrm{d}x$$

$$-\int_{x=a}^{x=b} \frac{1}{\sigma^2} \left(\frac{\partial p}{\partial z} + \frac{\mathrm{d}h}{\mathrm{d}x} \frac{\partial p}{\partial x} \right) \delta p \, \mathrm{d}x - \frac{1}{\sigma_1^2} \int_{z=-h_1}^{z=0} \left(\frac{\partial p}{\partial x} - \frac{\partial p^{(1)}}{\partial x} \right) \delta p \, \mathrm{d}z$$

$$+ \frac{1}{\sigma_3^2} \int_{z=-h_3}^{z=0} \left(\frac{\partial p}{\partial x} - \frac{\partial p^{(3)}}{\partial x} \right) \delta p \, \mathrm{d}z + \frac{1}{\sigma_1^2} \int_{z=-h_1}^{z=0} \left(p - p^{(1)} \right) \delta \left(\frac{\partial p^{(1)}}{\partial x} \right) \mathrm{d}z$$

$$- \frac{1}{\sigma_3^2} \int_{z=-h_3}^{z=0} \left(p - p^{(3)} \right) \delta \left(\frac{\partial p^{(3)}}{\partial x} \right) \mathrm{d}z = 0, \tag{3.2}$$

and the proof of the equivalence of (3.2) and the transmission problem (2.16) is finally obtained by using standard arguments of the calculus of variations. The present functional (3.1) and the variational principle (3.2) have been inspired by Chen & Mei (1974) and Bai & Yeung (1974), concerning wave–body interaction problems governed by the Laplace equation and characterized by complex boundaries, as reported in Mei (1983, §7.7), which has served as the basis for developing a hybrid element method. Furthermore, (3.1) and (3.2) reduce to the corresponding forms given in the above works if the current is zero. In the present work, the functional has been modified in order to make it suitable for scattering problems governed by (2.7a), that is essentially the modified Helmholtz equation with an additional first-order term modelling the effect of shear current on the wave field. However, in the present case the wave flow is not irrotational, and thus, a wave potential does not exist.

4. The coupled-mode system

In this section, we shall present a new coupled-mode system (CMS) modelling the scattering of waves by horizontal shearing current in variable bathymetry regions. The CMS is derived from the variational principle (3.2) using the following enhanced local-mode series representation of the wave pressure field in the variable bathymetry region $D^{(2)}$ (where also the current velocity $U(x)$ is varying):

$$p(x, z) = P_{-1}(x) Z_{-1}(z; x) + P_0(x) Z_0(z; x) + \sum_{n=1}^{\infty} P_n(x) Z_n(z; x). \tag{4.1}$$

This type of representation has been first introduced and studied by Athanassoulis & Belibassakis (1999) for the propagation of water waves over variable bathymetry

regions. In (4.1), the term $P_0(x) Z_0(z;x)$ is the propagating mode of the wave pressure field and the remaining terms $P_n(x) Z_n(z;x)$, $n = 1, 2, \ldots$ are the evanescent modes. The additional term $P_{-1}(x) Z_{-1}(z;x)$ is a correction term called the sloping-bottom mode, which properly accounts for the satisfaction of the bottom boundary condition on the sloping parts of the bottom, and identically vanishes on the horizontal parts of the bottom. The function $Z_n(z;x)$ represents the vertical structure of the nth mode. The function $P_n(x)$ describes the horizontal pattern of the nth mode and is called the complex amplitude of the nth mode.

The infinite set of functions $Z_n(z;x)$, $n = 0, 1, 2 \ldots$, appearing in (4.1) are obtained as the eigenfunctions of the following local vertical Sturm–Liouville problem,

$$\frac{\mathrm{d}^2 Z_n}{\mathrm{d}z^2} + \kappa_n^2 Z_n = 0 \qquad \text{in the interval} -h(x) < z < 0, \qquad (4.2a)$$

$$\frac{\mathrm{d}Z_n(z=0)}{\mathrm{d}z} - \mu(x) Z_n(z=0) = 0 \quad \text{at } z = 0. \qquad (4.2b)$$

$$\frac{\mathrm{d}Z_n(z=-h)}{\mathrm{d}z} = 0 \qquad \text{at } z = -h(x), \qquad (4.2c)$$

thus ensuring completeness of the expansion in the vertical direction. These are given by

$$Z_0(z;x) = \frac{\cosh[\kappa_0(x)(z+h(x))]}{\cosh(\kappa_0(x)\,h(x))}, \quad Z_n(z;x) = \frac{\cos[\kappa_n(x)(z+h(x))]}{\cos(\kappa_n(x)\,h(x))} \quad (n = 1, 2, \ldots), \qquad (4.3a)$$

where the eigenvalues $\{i\kappa_0(x), \kappa_n(x)\}$ are obtained as the roots of the local dispersion relation (formulated at the local depth $h(x)$ and for the local frequency parameter $\mu(x)$):

$$\mu(x) h(x) = -\kappa(x) h(x) \tan[\kappa(x)\,h(x)] \text{ in } a \leqslant x \leqslant b \text{ where } \mu(x) = \sigma^2(x)/g. \qquad (4.3b)$$

The modes $P_n Z_n, n = 0, 1, 2, \ldots$, satisfy (4.2c) at the bottom, which is different from the boundary condition (2.7c) on the non-horizontal parts of the bottom. This problem is remedied by the introduction of the extra sloping-bottom mode $P_{-1} Z_{-1}$. A specific convenient form of the function $Z_{-1}(z;x)$ associated with the latter mode is given by

$$Z_{-1}(z;x) = h(x)[(z/h(x))^3 + (z/h(x))^2], \qquad (4.4)$$

and all numerical results presented here are based on this choice. However, other choices are also possible (see Athanassoulis & Belibassakis 1999, §4). From (4.1), (4.2c) and (4.4), we easily find that the sloping-bottom mode satisfies:

$$P_{-1}(x) = \frac{\partial p\,(x, z = -h\,(x))}{\partial z}, \qquad (4.5)$$

and thus, it is needed only in subareas where the bottom surface is not flat. This additional mode makes the series (4.1) compatible with the Neumann bottom boundary condition (2.7c) in the sloping parts of the bottom surface, while, at the same time, it significantly accelerates the convergence of the local-mode series. For more details about the role and significance of this term, see Athanassoulis & Belibassakis (1999, §4), where this idea is first introduced and discussed for wave propagation/diffraction problems in variable bathymetry regions. Further details about the extension of this model to three dimensions can be found in Belibassakis, Athanassoulis & Gerostathis (2001).

The local-mode expansion (4.1) is developed in order to represent accurately and consistently the wave field (in the sense of completeness of the set of vertical eigenfunctions and taking care for the correct satisfaction of the boundary condition on the sloping bottom). Furthermore, each mode $P_n Z_n$, $n = -1, 0, 1, \ldots$, fulfils the homogeneous free-surface condition (2.7b), individually. Thus, the latter condition is satisfied as an essential one and, by using the present expansion in the variational equation, the latter is considerably simplified, since the second term on the left-hand side can be dropped. On the contrary, the field equation (2.7a) and the bottom-boundary condition (2.7c) are to be satisfied by the superposition of all modes, as calculated through the correct mode coupling that will be imposed by the final coupled-mode system. Finally, it must be remarked here that, the present expansion is physically consistent with the structure of the wave field in the case of a homogeneous environment (horizontal bed and uniform current). In that case, the sloping-bottom mode disappears (cf. (4.5)) and the rest of modes $P_n Z_n$, $n = 0, 1, \ldots$, satisfy (2.7) by themselves.

By using the local-mode series representation (4.1) in the variational principle (3.2), in a similar way as described in Athanassoulis & Belibassakis (1999, §5), the following coupled-mode system (CMS) with respect to the pressure mode amplitudes is obtained:

$$\sum_{n=-1}^{\infty} a_{mn}(x)\, P_n''\,(x) + b_{mn}(x)\, P_n'\,(x) + (c_{mn}(x) - a_{mn}q^2)P_n(x) = 0, \qquad (4.6)$$

in $a < x < b$, $m = -1, 0, 1, \ldots$, where a prime denotes differentiation with respect to x. The coefficients a_{mn}, b_{mn}, c_{mn}, $m, n = -1, 0, 1, 2, \ldots$, of the CMS (4.6) are given by

$$a_{mn} = \langle Z_n, Z_m \rangle = \int_{z=-h(x)}^{z=0} Z_n\,(z;x)\, Z_m\,(z;x)\,\mathrm{d}z, \qquad (4.7a)$$

$$b_{mn} = 2 \left\langle \frac{\partial Z_n}{\partial x}, Z_m \right\rangle + \frac{2q}{\sigma} \frac{\mathrm{d}U}{\mathrm{d}x} \langle Z_n, Z_m \rangle + \frac{\mathrm{d}h}{\mathrm{d}x} [Z_n Z_m]_{z=-h}, \qquad (4.7b)$$

$$c_{mn} = \langle \nabla^2 Z_n, Z_m \rangle + \left\langle \frac{2q}{\sigma} \frac{\mathrm{d}U}{\mathrm{d}x} \frac{\partial Z_n}{\partial x}, Z_m \right\rangle + \left[\left(\frac{\mathrm{d}h}{\mathrm{d}x} \frac{\partial Z_n}{\partial x} + \frac{\partial Z_n}{\partial z} \right) Z_m \right]_{z=-h}. \qquad (4.7c)$$

4.1. Boundary conditions for the CMS

The CMS (4.6) is supplemented by the following decoupled end-conditions at $x = a$ and $x = b$, which are obtained from the last four terms of the variational equation (3.2),

$$P_{-1}(a) = P_{-1}'(a) = 0, \quad P_{-1}(b) = P_{-1}'(b) = 0 \quad (n = -1), \qquad (4.8a)$$

$$P_0'(a) + \mathrm{i}k_0^{(1)} P_0(a) = 2\,\mathrm{i}k_0^{(1)}A_0 \exp\left(i\,k_0^{(1)}a\right), \quad P_n'(a) - k_n^{(1)} P_n(a) = 0 \quad (n = 1, 2, \ldots), \qquad (4.8b)$$

$$P_0'(b) - \mathrm{i}k_0^{(3)} P_0(b) = 0, \quad P_n'(b) + k_n^{(3)} P_n(b) = 0 \quad (n = 1, 2, \ldots), \qquad (4.8c)$$

where the coefficients $k_n^{(1)}$, $k_n^{(3)}$, $n = 0, 1, 2, \ldots$, are defined by (2.11a). The coefficients of the series expansions (2.10) in the two half-strips are obtained from the solution of the coupled-mode system through $P_n(a)$, $P_n(b)$, and are given by similar relations, as in Athanassoulis & Belibassakis (1999, (5.18)). In particular, the coefficients A_R and A_T defining the reflection and transmission coefficients

$$K_r = A_R/A_0, \quad K_t = A_T/A_0, \qquad (4.9a)$$

are obtained from the solution of the CMS (4.6) as follows:

$$A_R = \left(P_0(a) - A_0 \exp\left(ik_0^{(1)}a\right)\right) \exp\left(ik_0^{(1)}a\right), \quad A_T = P_0(b) \exp\left(-ik_0^{(3)}b\right). \quad (4.9b)$$

An important feature of the solution of the present scattering problem by means of the representation (4.1), is that it exhibits an improved rate of decay of the modal amplitudes $|P_n(x)|$ of the order $O(n^{-4})$. Thus, a small number of modes suffices to obtain a numerically convergent solution to $P(x, z)$, even for large bottom slopes and rapidly varying currents.

4.2. *Simplified forms of the CMS*

In the case of mild bottom topography and slow current variations, the evanescent modes $P_n, n = 1, 2, 3, \ldots$, producing localized second-order effects, can be approximately disregarded. Also, because of bottom mildness, the sloping-bottom mode ($n = -1$) can be neglected. In this case, the CMS (4.6) is simplified to the one-equation model

$$a_{00}(x)P_0''(x) + b_{00}(x)P_0'(x) + (c_{00}(x) - a_{00}q^2)P_0(x) = 0,$$

which, using the fact that $b_{00} = a_{00}' + (2q/\sigma)U' a_{00}$, can be put into the following equation, which is called the *mild-slope and shear* equation:

$$(\alpha(x) P_0'(x))' + \frac{2qU'(x)\alpha(x)}{\sigma(x)} P_0'(x) + \left(\alpha(\kappa_0^2 - q^2) - K(x)\right) P_0(x) = 0. \quad (4.10)$$

The coefficients of (4.10) are given by

$$\alpha = a_{00} = \int_{z=-h(x)}^{z=0} Z_0^2(z;x)\, dz = \frac{1}{2\kappa_0} \tanh(\kappa_0 h)\left(1 + \frac{2\kappa_0 h}{\sinh(2\kappa_0 h)}\right), \quad (4.11a)$$

$$K(x) = -\int_{z=-h(x)}^{z=0} \frac{\partial^2 Z_0(z;x)}{\partial x^2} Z_0(z;x)\, dz - h'\left[\frac{\partial Z_0}{\partial x} Z_0\right]_{z=-h(x)}$$

$$+ \frac{2qU'}{\sigma} \int_{z=-h(x)}^{z=0} \frac{\partial Z_0(z;x)}{\partial x} Z_0(z;x)\, dz$$

$$= \beta(x) - \gamma'(x)/2 + qU'(x)\gamma(x)/\sigma(x), \quad (4.11b)$$

where

$$\beta = (24\kappa_0^3 \cosh \kappa_0 h)^{-1}(\nu_1(h')^2 + \nu_2(\kappa_0'h') + \nu_3(\kappa_0')^2),$$
$$\nu_1 = 6\kappa_0^4(2\kappa_0 h + \sinh \kappa_0 h),$$
$$\nu_2 = 6\kappa_0^3 h((-3 + \cosh 2\kappa_0 h)\kappa_0 h + \sinh 2\kappa_0 h),$$
$$\nu_3 = -6\kappa_0 h \cosh^2 \kappa_0 h + 4(-2 + \cosh 2\kappa_0 h) + 6 \cosh^3 \kappa_0 h \sinh \kappa_0 h,$$

and finally

$$\gamma = (\alpha' - h'/\cosh^2(\kappa_0 h)).$$

In the above equations, $Z_0(z;x)$ is given by (4.3a) and κ_0 is the positive root of the dispersion relation $\mu h = \kappa_0 \tanh(\kappa_0 h)$, equation (4.3b) for $n = 0$. From the latter, the derivative κ_0' is calculated to be: $\kappa_0' = (4(q^2U - 2\omega q)U' \cosh^2(\kappa_0 h) - 2\kappa_0^2 gh') \times (g\sin(2\kappa_0 h) - 2g\kappa_0 h)^{-1}$. In order to illustrate the richness and validity of the present model, we will now discuss two particular forms to which (4.10) reduces, when there is no current and when the bottom is horizontal.

(i) *No current* ($U = 0$)

In the case of wave scattering by bottom topography without current, (4.10) reduces exactly to the modified mild-slope equation (MMS) (Massel 1993; Chamberlain & Porter 1995),

$$(\alpha(x)P_0'(x))' + (\alpha(\kappa_0^2 - q^2) - K(x))P_0(x) = 0, \qquad (4.12a)$$

where

$$K(x) = -\int_{z=-h(x)}^{z=0} \frac{\partial^2 Z_0(z;x)}{\partial x^2} Z_0(z;x)\,\mathrm{d}z - h'\frac{\partial Z_0(z = -h(x);x)}{\partial x} = K_1 h'' + \kappa_0 K_2 (h')^2, \qquad (4.12b)$$

and K_1, K_2 are functions of $\kappa_0 h$, as given by Miles & Chamberlain (1998, equations (1.14b, c)).

(ii) *Scattering by shear current in flat domain* ($\mathrm{d}h/\mathrm{d}x = 0$)

In the case of a horizontal bottom, (4.10) can be written in the following form:

$$(\Gamma(x)P_0'(x))' + (\Gamma(x)(\kappa_0^2(x) - q^2) + \Lambda(x))P_0(x) = 0, \qquad (4.13a)$$

where

$$\Gamma(x) = (\sigma/\omega)^{-2} a_{00}(x), \quad \Lambda(x) = \left(\frac{\sigma}{\omega}\right)^{-2}\left(-\frac{2q}{\sigma}\frac{\mathrm{d}U}{\mathrm{d}x}\left\langle\frac{\partial Z_0}{\partial x}, Z_0\right\rangle + \left\langle\frac{\partial^2 Z_0}{\partial x^2}, Z_0\right\rangle\right). \qquad (4.13b)$$

Equation (4.13) is the enhanced mild-shear equation (EMSE), which has been derived and studied by McKee (1996). Furthermore, on the basis of very slow current variations ($|\mathrm{d}U/\mathrm{d}x| \ll 1$), the coefficient $\Lambda(x)$ becomes of higher order in comparison with $\kappa_0^2 \Gamma(x)$ and can be approximately neglected ($\Lambda(x) \approx 0$). In this case, (4.13) further reduces to the mild-shear equation (MSE), which has also been derived and studied by McKee (1987).

In order to investigate the validity of EMSE and MSE models, in constant-depth regions, McKee (2003) has developed an 'exact' multidomain approximation method, which is based on piecewise constant approximation of the current velocity and on complete normal-mode expansions (of the form of our (2.10)) in each subdomain. The final solution concerning the coefficients of these expansions is obtained by satisfying the matching conditions at the vertical interfaces (vortex sheets) separating each subdomain (see, e.g. Smith 1983, equations (2.3–2.4); Kirby *et al.* 1987, equations (2.13–2.14). As illustrated in §5.1 (below), the present CMS (4.6) results are found to be in perfect compatibility with the multidomain approximation method.

5. Numerical results and discussion

Here, we present numerical results obtained by the present CMS and by comparisons with other models. The discrete system is obtained by truncating the local-mode series (4.1) to a finite number of terms, retaining a number M of evanescent modes, in addition to the propagating and the sloping-bottom modes, and by using central second-order finite differences based on a uniform horizontal grid of N_p points to approximate the (horizontal) derivatives in (4.6). Discrete boundary conditions are obtained from (4.8) by using second-order forward and backward differences to approximate derivatives at the ends ($x = a$ and $x = b$). Thus, the discrete scheme is uniformly of second-order in the horizontal direction. The forcing due to the incoming
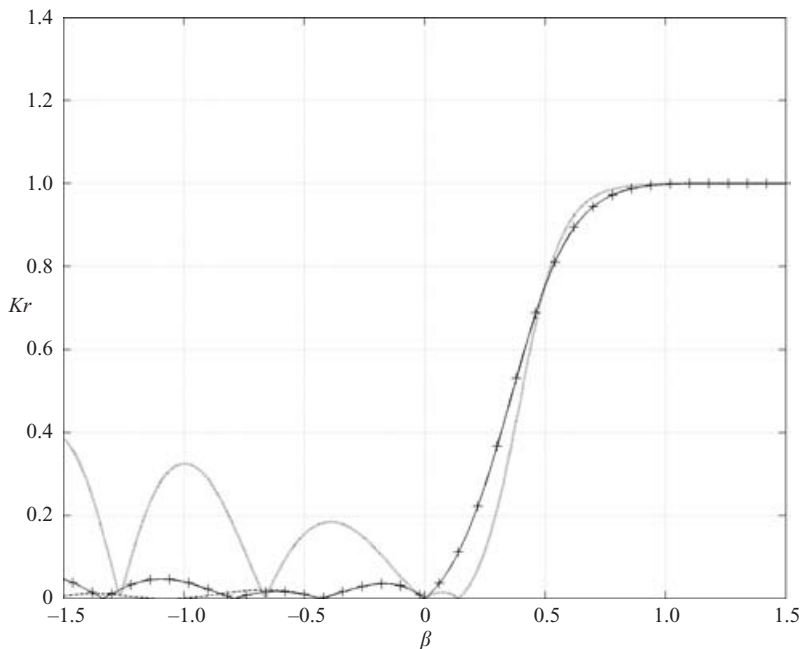
FIGURE 2. Obliquely incident waves scattered by opposing and following jet-like shear current, in deep water. Comparison of the reflection coefficient, as obtained by the present CMS (solid line), EMSE (dashed line) and MSE (dotted line), for various current velocities. +, results obtained by the multidomain approximation method (McKee 2003). $\theta_1 = 45°$; $\varepsilon = \omega^2 \ell / g = 1$; $S = \omega^2 h / g = 1$.

wave appears only in one equation, at the left endpoint $x = a$ (see (4.8b)). We note here that in all numerical examples presented and discussed in this section, the wave action conservation equations, (2.15), are fulfilled with (numerical) error less than 0.01%.

5.1. *Scattering of water waves by jet-like shear currents in constant depth*

We first consider the case of obliquely incident waves ($\theta_1 = 45°$), in constant depth ($h = \text{const}$), scattered by a jet-like current of the form:

$$U(x) = U_{max} \exp(-(x/\ell)^2). \tag{5.1}$$

To model the above shear current profile, we use $a = -3\ell$, $b = 3\ell$ and $U_1 = U_3 = 0$. In this example taken from McKee (2003), apart from the incidence wave direction (θ_1), the other important non-dimensional parameters are: $\varepsilon = \omega^2 \ell / g$, $\beta = U_{max} \omega / g$, $S = \omega^2 h / g$.

In figure 2, we present results concerning the reflection coefficient for $S = 1$ (deep-water conditions), $\varepsilon = 1$ and various maximum current velocities U_{max}, corresponding to β in the range $-2 < \beta < 2$, where negative values are associated with adverse currents and positive values with following currents, respectively. The present CMS results (shown by a solid line) have been obtained by using a total of 5 modes ($n = 0$, 1, 2, 3, 4), which were found to be enough for numerical convergence. We recall here that in constant depth, the sloping-bottom mode is zero by definition (see (4.5)) and need not be considered. The present CMS results are found to be in perfect agreement with those obtained by the multidomain approximation method (McKee 2003), shown also in figure 2 by crosses. In addition, in this figure we include the predictions for the reflection coefficient by EMSE (dashed line) and MSE (dotted line), respectively,
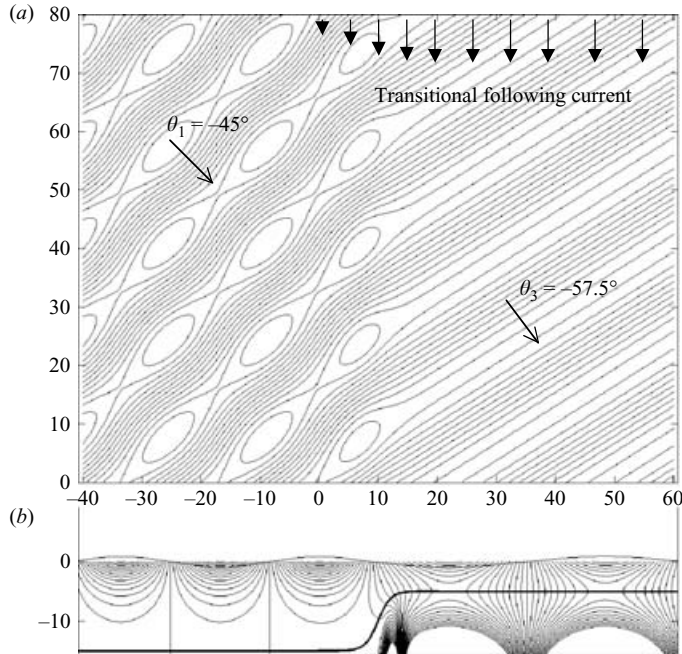
FIGURE 3. Refraction/diffraction of waves over a smooth and steep shoal, with the effects of a following transitional shear current. Plot of the wave field (a) on the horizontal plane, (b) on the vertical plane.

as calculated by the present method, using only the propagating mode ($n = 0$) and, in addition, by disregarding $\Lambda(x)$ in (4.13a). We can see in figure 2 the enhanced performance of the EMSE vs. the MSE model, as also reported by McKee (2003). In the case examined, the EMSE model accurately predicts the reflection coefficient for $\beta > -0.5$, i.e. for relatively weak adverse currents and for following currents.

5.2. Waves scattered by a smooth underwater shoal in the presence of a shear current

In order to illustrate the combined effects of variable bathymetry and shearing current on the wave field, we examine in this section the case of a smooth but steep underwater shoal, characterized by the following depth function

$$h(x) = \frac{h_1 + h_3}{2} - \frac{h_1 - h_3}{2} \tanh\left(3\pi\left(\frac{x - a}{b - a} - \frac{1}{2}\right)\right), \qquad (5.2)$$

in $a = 0 < x < b = 20\,\text{m}$, with $h_1 = 15\,\text{m}$ and $h_3 = 5\,\text{m}$. This bottom profile is quite steep, having mean slope 50 % and maximum slope 240 %. (A sketch of the bottom topography is shown in figures 3 and 4). The angular frequency of the incident wave is selected to be $\omega = 1.62\,\text{rad}\,\text{s}^{-1}$, corresponding to shoaling ratio $h_1/\lambda = 0.64$, where λ is the local wavelength (that implies almost deep-water-wave conditions in $D^{(1)}$), and the incident wave direction is taken to be $\theta_1 = -45°$. The phase speed of the waves in the region of incidence is $c_1 = 6.06\,\text{m}\,\text{s}^{-1}$.

We first consider the case of wave scattering by bottom topography only, without any current effects. In this case, the shoaling ratio is $h_3/\lambda = 0.235$ (implying intermediate water-depth wave conditions in $D^{(3)}$), and the corresponding phase speed of the waves in the region of transmission is $c_3 = 5.47\,\text{m}\,\text{s}^{-1}$. After passing
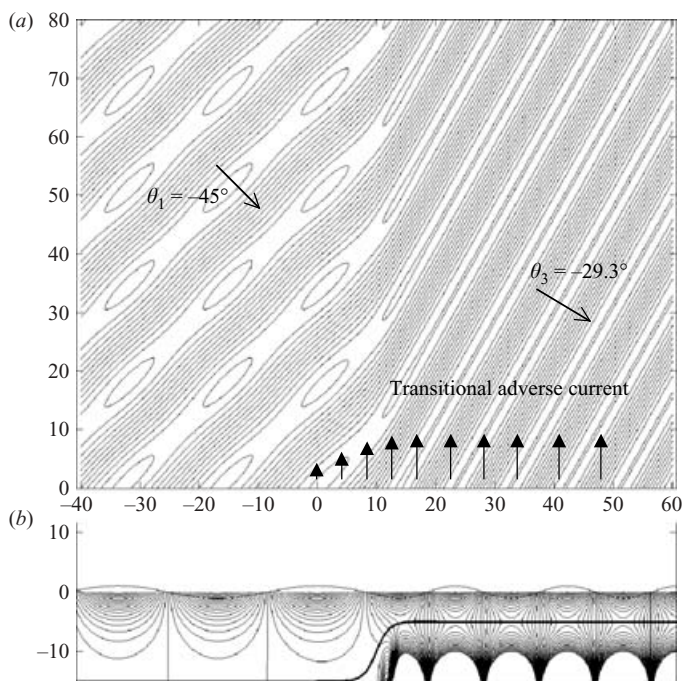
FIGURE 4. Refraction/diffraction of waves over a smooth and steep shoal, with the effects of an opposing transitional shear current. Plot of the wave field (*a*) on the horizontal plane, (*b*) on the vertical plane.

through the variable bathymetry region, the waves are refracted owing to shoaling and the direction of the transmitted wave is $\theta_3 = -39.6°$. In this case, the reflection and transmission coefficients, as calculated by the present CMS (4.6) using a total of 5 modes ($n = -1, 0, 1, 2, 3$) and $N_p = 251$, are found to be: $K_r = 0.025$, $K_t = 0.884$. In this and similar cases that will be presented in the sequel, such a small number of retained modes in the local-mode series (4.1) is found to be enough for numerical convergence, provided that the sloping-bottom mode ($n = -1$) is included. We remark here that in the case of no current, the present CMS becomes equivalent to the consistent coupled-mode model developed by Athanassoulis & Belibassakis (1999) for the propagation of waves over variable bathymetry regions.

In figures 3 and 4, we present results for the same shoal and wave incidence as before, but with the additional effects of a following (figure 3) and of an opposing (figure 4) transitional shear current. In this case, the current velocity profile is taken to be given by

$$U(x) = \frac{U_3}{2} + \frac{U_3}{2} \tanh\left(3\pi\left(\frac{x-a}{b-a} - \frac{1}{2}\right)\right), \qquad (5.3)$$

in $a = 0 < x < b = 20$ m. Thus, the shear current velocity varies monotonically from a minimum value $U_1 = 0$ to a maximum value U_3, which is taken to be a quarter of the phase speed of waves in the region of incidence, $U_3 = \max U = 0.25c_1$ (where $c_1 = 6.06 \text{ m s}^{-1}$). Now, the wave directions in the region of transmission $D^{(3)}$ are modified owing to current, and in the case of the following current, $|\theta_3|$ increases, whereas in the case of the adverse current, $|\theta_3|$ decreases, as predicted by (2.14).

Contour plots of the wave field (real part of wave pressure) above the variable bathymetry domain are shown in figures 3 and 4, respectively. In these figures, the

Current type	max U/c_1	$|\theta_3|$	K_r	K_t
–	0	39.6	0.025	0.884
Following	0.25	57.5	0.176	0.852
Opposing	−0.25	29.3	0.053	0.999

TABLE 1. Refraction/diffraction parameters of waves scattered by transitional shearing current over smooth underwater shoal.

system of isobars is shown both in the horizontal plane (upper part of the figures) and in the vertical plane (lower part). The direction and horizontal structure of the current is also schematically shown in these figures by using arrows. Extension of the isobars below the bottom surface has been maintained in the lower part of this figure in order to visualize better the fulfilment of the Neumann boundary condition on $z = -h(x)$, which is equivalent to the fact that the equipressure lines intersect the bottom profile perpendicularly (cf. (2.7c)). Also, the distribution of the wave pressure on the free surface is plotted in figures 3(b) and 4(b), which is proportional to the free-surface elevation (equation (2.8)). We observe in these figures, the continuous variation of the wavelength (which increases for following and decreases for adverse currents), taking place in the intermediate subdomain $D^{(2)}$. The main results concerning the refraction parameters, reflection and transmission coefficients are summarized in table 1.

5.3. The case of a sinusoidal current

It is well known that in the case of obliquely incident waves on an opposing jet-like shear current, in constant depth, wave trapping can occur under particular conditions (see, e.g. the discussion by Mei 1983, §3.7.2 and figure 7.2, and the discussion after equation (6.22)). This could lead to great amplification of the wave in a transverse channel along the current maximum. On the other hand, observations suggested that wind-wave amplitudes might be enhanced within the downwind-directed current maxima associated with alternating 'wind streaks' or 'Langmuir circulation' (see also Smith 2001), leading to preferential breaking of waves along such current jets. In order to investigate such phenomena theoretically, Smith (1983) developed an eigenfunction expansion technique for the scattering of waves in constant depth by narrow current jets, modelled by a top-hat pattern. The model problem consisted of three homogeneous subregions separated by vertical vortex sheets. However, the results indicated that wave amplitudes should be decreased within such current jets.

In order to extend the previous investigation, which was restricted to single uniform current jets and shear concentrated along the edges of the jet, to the case of more complex, horizontally alternating current structure, we consider here as another example the case of waves of angular frequency $\omega = 2.2\,\text{rad s}^{-1}$, propagating with direction $\theta_1 = 60°$ in a constant depth strip $h = 15\,\text{m}$, and scattered by a following sinusoidal shear current with horizontal profile of the form:

$$U(x) = \frac{U_{max}}{2}\left(1 - \cos\left(2\pi\frac{x-a}{L}\right)\right), \qquad L = \frac{b-a}{2}, \tag{5.4}$$

taking the maximum current velocity U_{max} to be equal to a tenth of the phase speed of waves in $D^{(1)}$ and $D^{(3)}$, which in the present case is $c_1 = c_3 = 4.46\,\text{m s}^{-1}$. This current has the form of two streaks and is characterized by continuously distributed shear. More specifically, the shear current exists only in the region from $a = 0\,\text{m}$ to $b = 20\,\text{m}$ ($U_1 = U_3 = 0$), and it has a periodic horizontal structure with characteristic length $L = 10\,\text{m}$, that is comparable to the incident wavelength ($L/\lambda = 0.78$). In addition,
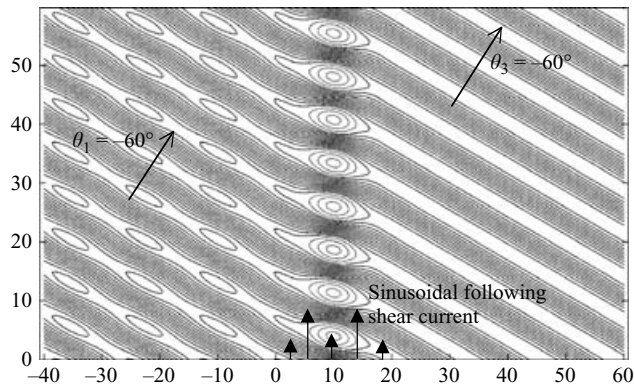
FIGURE 5. Refraction/diffraction of waves by a following sinusoidal current, in constant depth. Plot of the wave field on the horizontal plane.
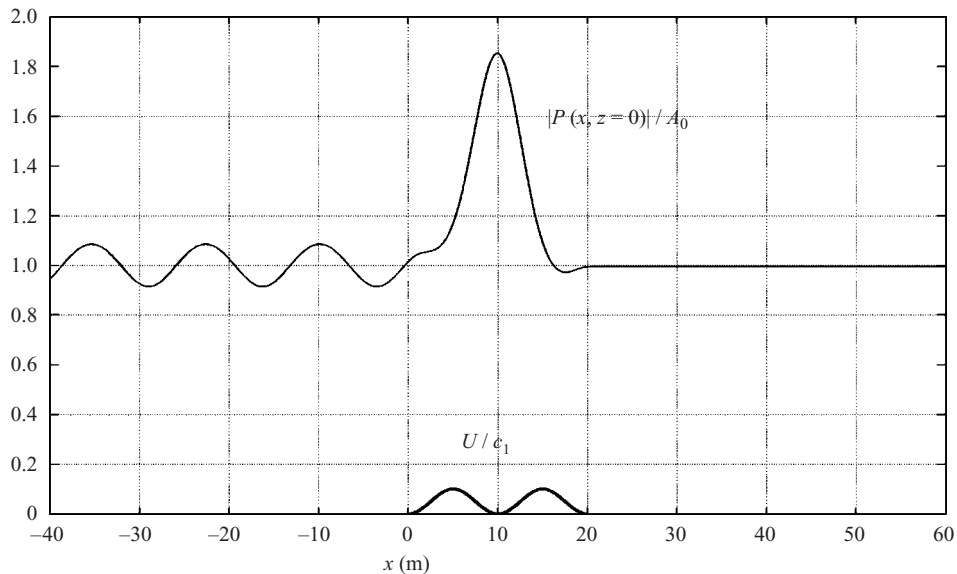

FIGURE 6. Amplification factor of waves scattered by a following sinusoidal current. Incident wave frequency $\omega = 2.2 \, \text{rad s}^{-1}$ and direction $\theta_1 = 60°$.

the wave conditions in the region of incidence correspond to deep-water conditions ($h/\lambda = 1.17$).

The real part of the calculated wave field is shown in figure 5, as obtained by the present method by using only 5 modes ($n = 0, 1, 2, 3, 4$) in the series (4.1) and $N_p = 251$. Again, the latter have been proved to be enough for numerical convergence, even for such large gradients of the horizontal current velocity. We observe in figure 5 the formation of a transverse channel on the horizontal plane, centred at $x = 10$ m, associated with partial trapping of the wave energy.

In figure 6, we present the amplification factor of the wave $|P(x, z = 0)|/A_0$ (where A_0 is the amplitude of the incident wave), as calculated by the present method, along with the sinusoidal current profile. Strong enhancement of the wave amplitude is

observed at $x = 10\,\text{m}$, i.e. along the central axis of the current (5.4), corresponding to more than an 80% increase of the incident wave amplitude.

An explanation of this result is possible on the basis of simple refraction principles. The incident wave direction increases within the first current jet ($0 < x < 10\,\text{m}$) owing to increase of phase speed (Mei 1983, figure 7.2a). Because the wavelength is comparable with the horizontal length of the current, the wave at the exit of the first jet ($x = 10\,\text{m}$) has a local direction which is greater than $60°$. The latter is such that the wave is partially reflected from the second jet (Mei 1983, figure 7.2b). Thus, a small part of wave energy returns towards the central axis of the current and is trapped in the transverse channel. The calculated reflection and transmission coefficients by the present CMS are: $K_r = 0.085$, $K_t = 0.996$. Thus, almost all the wave energy penetrates the region of transmission $D^{(3)}$, and at $x > 20\,\text{m}$ the wave direction has recovered its initial value: $\theta_3 = \theta_1 = 60°$. Consequently, repeated similar patterns of wave enhancement are expected to occur, if the alternating following current structure (5.4) is assumed to be periodically extended in $D^{(3)}$.

5.4. *Longshore current effects on resonant reflection of waves by sinusoidal bathymetry*

A final result presented in this work concerns the investigation of longshore current effects on the reflection of waves by sinusoidal bathymetry. The phenomenon of resonant reflection by undulating bottom topography has drawn considerable attention owing to its significant role in the evolution of nearshore waves and its possible relation to coastal morphology (development of shore-parallel bars). In addition, the existence of Bragg scattering provides a possible means for constructing coastal protection devices relatively low in profile in comparison to the waterdepth. The above remarks justify the extent of theoretical and experimental works presented on this subject by many authors (see, for example, Davies & Heathershaw 1984; Mei 1985; Mei, Hara & Naciri 1988; Guazzelli, Rey & Belzons 1992; Kirby 1993; O'Hare & Davies 1993; Liu & Yue 1998).

However, as pointed out by Kirby (1988), any such physical formation or installation is of finite length along the longshore dimension. This is likely to result in depression of the maximum set-up behind the bar which would generate a nearshore circulation pattern. This is expected to produce mean flows with onshore/offshore directions, and perhaps also with a longshore component above the bar field. The effects of cross-shore current on the resonant reflection of water waves by sand bars have been studied by Kirby (1988), by using multiple-scale expansions to obtain evolution equations for the amplitudes of waves. The latter were then used to investigate the resonant reflection of waves by bar fields for both normal and oblique incidence. In order to examine the longshore shear current effects on resonant reflection of waves by sinusoidal bathymetry using the present CM, we consider the bottom topography characterized by the following depth function:

$$h(x) = h_0 - B \sin(\ell_b x) \quad \text{in} \quad 2\pi/\ell_b < x < 2\pi(n+1)/\ell_b; \quad h(x) = h_0 \text{ otherwise. (5.5)}$$

In (5.5), ℓ_b denotes the bottom wavenumber and B the amplitude of the bottom undulations. To maintain correspondence with the experimental results presented in Davies & Heathershaw (1984), $n = 4$ case, we chose $h_0 = 15.625\,\text{cm}$, $B/h_0 = 0.32$ and $\ell_b = 2\pi$ (so that the length of the bottom periodic cell is 1 m). Numerical results are obtained by the present CMS using a total of 5 modes ($n = -1, 0, 1, 2, 3$) and 251 gridpoints per bottom wavelength. The results concerning the reflection coefficient are shown in figure 7 for values of the resonant parameter $0.5 < 2\kappa \cos(\theta)/\ell_b < 1.8$, around the point of first-order Bragg resonance. The latter in the case of no current
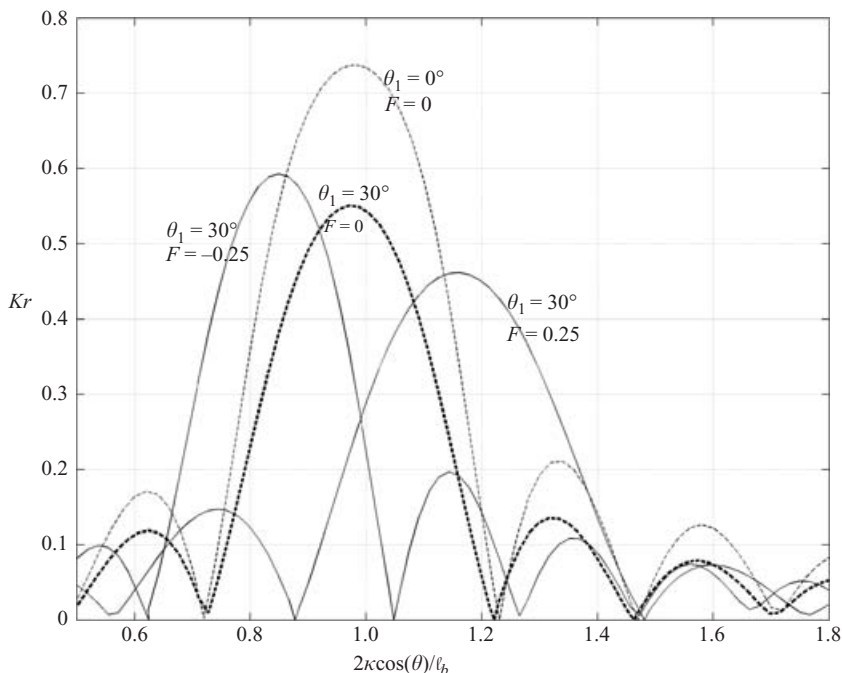
FIGURE 7. Wave reflection over sinusoidal bottom topography for various incidence angles θ_1 and bathymetric Froude numbers F.

is defined by

$$2\kappa \cos(\theta)/\ell_b = 1, \tag{5.6}$$

where in this subsection κ and θ will be used to denote the incident wavenumber and direction ($\kappa = \kappa_0^{(1)}$ and $\theta = \theta_1$). For comparison, in figure 7 we present results (always obtained by the present CMS) for normal $\theta = 0°$ and oblique $\theta = 30°$ incidence, without current (shown by dashed lines), and for oblique incidence $\theta = 30°$ with the effects of following and opposing jet-like currents. The current profile is of the form of (5.4), with $L = b - a$ and $a = 0$ m, $b = 6$ m. In order to illustrate the current effects better, relatively strong velocities have been considered, corresponding to bathymetric Froude numbers $F = U_{max}/\sqrt{gh_0} = \pm 0.25$.

In the case of no current, the results of the present method, shown by dashed lines in figure 7, are found to be in very good agreement with corresponding predictions by other theoretical models and with experimental data; cf. O'Hare & Davies (1993, figure 3*b*), in the case of normal incidence, and Kirby (1993, figure 5), in the case of oblique incidence. We observe in figure 7 that the peak of the main lobe of the reflection coefficient (K_r) is located at $2\kappa \cos(\theta)/\ell_b \approx 0.98$, i.e. slightly shifted to a lower value of the resonance parameter than that predicted by (5.6).

The Doppler shift of frequency owing to the current, also shifts the position of the peak of the main lobe of K_r from $2\kappa \cos(\theta)/\ell_b \approx 1$, for $F = 0$, to a much lower value $2\kappa \cos(\theta)/\ell_b \approx 0.84$ in the case of opposing current ($F = -0.25$), and to a higher value $2\kappa \cos(\theta)/\ell_b \approx 1.16$ in the case of following current ($F = 0.25$). The above differences (-0.14 and 0.18, respectively) in the values of the resonant parameter $2\kappa \cos(\theta)/\ell_b$ controlling the location of the main the peak of K_r can be predicted, at a first order of approximation, by using the dispersion relation formulated at $F = 0$ to obtain the

variation of wavenumber in the neighbourhood of the K_r-peak due to frequency shift:

$$\Delta\kappa = \frac{1}{C_g}(\sigma - \omega) = -\frac{q U_{max}}{C_g} = -\frac{\kappa \sin(\theta) U_{max}}{C_g}, \qquad (5.7)$$

where $C_g = \mathrm{d}\omega/\mathrm{d}k$ denotes the group velocity calculated at $\kappa = \ell_b/2\cos(\theta)$ without taking into account any current effects. Using (5.7) for $\kappa = \ell_b/2\cos(\theta)$, in conjunction with the resonance condition, which now reads

$$2(\kappa + \Delta\kappa)\cos(\theta)/\ell_b = 1, \qquad (5.8)$$

we obtain

$$2\kappa\cos(\theta)/\ell_b = 1 \pm \varepsilon. \qquad (5.9a)$$

In (5.9a) the plus sign refers to a following current and the minus sign to an opposing current, respectively, and here

$$\varepsilon = \frac{2|\Delta\kappa|\cos(\theta)}{\ell_b} = \frac{2\sin(\theta)F}{P}\left(\frac{2\cos(\theta)}{\ell_b h}\tanh\left(\frac{\ell_b h}{2\cos(\theta)}\right)\right)^{-1/2}, \qquad (5.9b)$$

$$\text{where } P = 1 + \frac{\ell_b h/\cos(\theta)}{\sinh(\ell_b h/\cos(\theta))}.$$

Application of (5.9b) to the examined case results in $\varepsilon = 0.145$. Thus, (5.9) predicts the location of the main-lobe peak at $2\kappa\cos(\theta)/\ell_b = 1 \pm 0.145$ which is found to approximate well the real values 0.84 and 1.16, respectively.

Furthermore, we observe in figure 7 that in the examined wave incidence $\theta = 30°$, the shape of the main lobe of K_r for $F = \pm 0.25$ looks similar to that for $F = 0$. However, the main lobe is ∼9 % narrower in the case of an opposing current, and ∼19 % broader in the case of a following current, in comparison with the no current case ($F = 0$). Also, the peak value of K_r appears to be ∼10 % greater for $F = -0.25$, and ∼18 % lower for $F = 0.25$. Thus, it seems that the area under the main lobe of the reflection coefficient is approximately conserved for symmetric jet-like currents. The above results and remarks may be useful for extending analytical models for the approximate prediction of the reflection coefficient around the position of the peak of the main lobe (as e.g. those given by Mei *et al.* 1988; Kirby 1993) to the case of Bragg scattering by a sinusoidal bottom in the presence of longshore shear currents, at least for low angles of wave incidence where the K_r pattern is less complex (see, e.g. Kirby 1993, figure 5).

6. Conclusions

A continuous coupled-mode method has been developed for wave–current–seabed interaction in variable bathymetry regions, with application to the problem of wave scattering by steady shearing currents, characterized by current variations on various scales. The present method does not introduce any simplifying assumptions or other restrictions concerning the bottom slope and curvature or the horizontal gradient of the current. Based on a variational principle, in conjunction with a rapidly convergent local-mode series expansion of the wave pressure field in a finite subregion containing the current variation and the bottom irregularity, a new coupled-mode system of equations is obtained, governing the scattering of waves in the presence of variable bathymetry and longshore shearing currents. In addition, by keeping only the propagating mode in the local-mode series, a new one-equation model has been derived, called the *mild slope and shear equation*, having the property to reduce to

modified mild-slope equation when the current is zero and to the enhanced mild-shear equation when the bottom is flat. Finally, the analytical structure of the present model facilitates its extension in various directions as: (i) to three-dimensional problems; (ii) to treat wave scattering by more complex current systems, characterized by more general vertical structure with cross-jet component; and (iii) to include the effects of weak nonlinearity.

REFERENCES

ATHANASSOULIS, G. A. & BELIBASSAKIS, K. A. 1999 A consistent coupled-mode theory for the propagation of small-amplitude water waves over variable bathymetry regions. *J. Fluid. Mech.* **389**, 275–301.

BAI, K. J. & YEUNG, R. W. 1974 Numerical solution to free-surface flow problems. *Proc. 10th Naval Hydrodyn. Symp.* Office of Naval Research, Cambridge, MA.

BELIBASSAKIS, K. A., ATHANASSOULIS, G. A. & GEROSTATHIS, TH. 2001 A coupled-mode model for the refraction–diffraction of linear waves over steep three-dimensional bathymetry. *Appl. Ocean Res.* **23**, 319–336.

BERKHOFF, J. C. W. 1972 Computation of combined refraction–diffraction. *Proc. 13th Intl Conf. on Coastal Engineering*, pp. 796–814. ASCE.

CHAMBERLAIN, P. G. & PORTER, D. 1995 The modified mild-slope equation. *J. Fluid Mech.* **291**, 393–407.

CHEN, H. S. & MEI, C. C. 1974 Oscillations and wave forces in a man-made harbor in the open sea, *Proc. 10th Naval Hydrodyn. Symp.* Office of Naval Research, Cambridge, MA.

CHEN, W., PANCHANG, V. & DEMIRBILEK, Z. 2005 On the modeling of wave–current interaction using the elliptic mild-slope wave equation. *Ocean Engng* **32**, 2135–2164.

DAVIES, A. G & HEATHERSHAW, A. D. 1984 Surface-wave propagation over sinusoidal varying topography. *J. Fluid Mech.* **144**, 419–433.

DYSTHE, K. B. 2000 Modelling a rogue wave – speculations or a realistic possibility. In *Rogue Waves 2000* (ed. M. Olagnon & G. Athanassoulis), pp. 255–264. Editions Ifremer, Plouzane, France.

EVANS, D. V. 1975 The transmission of deep-water waves across a vortex sheet. *J. Fluid Mech.* **68**, 389–401.

FAULKNER, D. 2000 Rogue waves – defining their characteristics for marine design. In *Rogue Waves 2000* (ed. M. Olagnon & G. Athanassoulis), pp. 3–18. Editions Ifremer, Plouzane, France.

GUAZZELI, E., REY, V. & BELZONS, M. 1992 Higher-order Bragg reflection of gravity surface waves by periodic beds *J. Fluid Mech.* **245**, 301–317.

JONSSON, I. G. 1990 Wave–current interactions. In *The Sea* (ed. B. LeMehaute & D.M. Hanes), pp. 65–120. John Wiley.

KIRBY, J. T. 1984 A note on linear surface wave–current interaction over slowly varying topography. *J. Geophys. Res.* **89**, 745–74.

KIRBY, J. T. 1988 Current effects on resonant reflection of surface water waves by sand bars. *J. Fluid Mech.* **186**, 501–520.

KIRBY, J. T. 1993 A note on Bragg scattering of surface waves by sinusoidal bars. *Phys. Fluids* A **5**, 380–386.

KIRBY, J. T., DALRYMPLE. R. A. & SEO, S. N. 1987 Propagation of obliquely incident water waves over a trench. Part 2. Currents flowing along the trench. *J. Fluid Mech.* **176**, 95–116.

LIU, P. L.-F. 1990 Wave transformation. In *The Sea* (ed. B. LeMehaute & D. M. Hanes), pp. 27–63. John Wiley.

LIU, Y. & YUE, D. K. P. 1998 On generalized Bragg scattering of surface waves by bottom ripples. *J. Fluid Mech.* **356**, 297–326.

MCKEE, W. D. 1987 Waver waves propagation across a shearing current. *Wave Motion.* **9**, 209–215.

MCKEE, W. D. 1996 A model for surface wave propagation across a shearing current. *J. Phys. Oceanogr.* **26**, 276–278.

MCKEE, W. D. 2003 The propagation of water waves across a shearing current. *Rep. Dept of Appl. Math., Univ. of New South Wales* AMR 03/26.

MASSEL, S. R. 1993 Extended refraction–diffraction equation for surface waves. *Coastal Engng* **19**, 97–126.

Mei, C. C. 1983 *The Applied Dynamics of Ocean Surface Waves.* John Wiley (2nd Reprint, 1994, World Scientific).

Mei, C. C. 1985 Resonant reflection of surface water waves by periodic sand-bars.*J. Fluid Mech.* **152**, 315–335.

Mei, C. C., Hara, T. & Naciri, M. 1988 Note on Bragg scattering of water waves by parallel bars on the seabed. *J. Fluid Mech.* **186**, 147–162.

Miles, J. W. & Chamberlain, P. G. 1998 Topographical scattering of gravity waves. *J. Fluid Mech.* **361**, 175–188.

O'Hare, T. J. & Davies, A. G. 1993 A comparison of two models for surface-wave propagation over rapidly varying topography. *Appl. Ocean Res.* **15**, 1–11.

Peregrine, D. H. 1976 Interaction of waves and currects. *Adv. Appl. Mech.* **16**, 9–17.

Smith, J. 1983 On surface gravity waves crossing weak current jets. *J. Fluid Mech.* **134**, 277–299.

Smith, J. 1987 On surface waves crossing a step with horizontal shear. *J. Fluid Mech.* **175**, 395–412.

Smith, J. 2001 Observations and theories of Langmuir circulation: a story of mixing. In *Fluid Mechanics and the Environment: Dynamical Approaches* (ed. J. L. Lumney). Springer.

Thomas, G. P. & Klopman, G. 1997 Wave–current interaction in the nearshore region. In *Gravity Waves in water of Finite Depth* (ed. J. N. Hunt). Computational Mechanics Publications.